Inhibitory SMAD6 interferes with BMP-dependent generation of muscle progenitor cells and perturbs proximodistal pattern of murine limb muscles

Hasan A. Asfour, Estelle Hirsinger, Raquel Rouco, Faouzi Zarrouki, Shinichiro Hayashi, Sandra Swist, Thomas Braun, Ketan Patel, Frédéric Relaix, Guillaume Andrey, et al.

Title: Inhibitory SMAD6 interferes with BMP dependent generation of muscle progenitor cells and perturbs proximodistal pattern of murine limb muscles.

Authors

Hasan Asfour[1], Estelle Hirsinger[2], Raquel Rouco[3], Faouzi Zarrouki[1], Shinichiro Hayashi[4], Sandra Swist[5], Thomas Braun[5], Ketan Patel[6], Frédéric Relaix[7], Guillaume Andrey[3], Sigmar Stricker[8], Delphine Duprez[2], Amalia Stantzou[1,*], Helge Amthor[1,9,*]

Affiliations

[1] Université Paris-Saclay, UVSQ, Inserm, END-ICAP, 78000 Versailles, France.
[2] Sorbonne Université, Institut Biologie Paris Seine, CNRS UMR7622, Developmental Biology Laboratory, Inserm U1156, 75005 Paris, France.
[3] University of Geneva, Faculty of Medicine, Department of Genetic Medicine and Development, 1211 Geneva 4, Switzerland.
[4] National Center of Neurology and Psychiatry (NCNP), National Institute of Neuroscience, Department of Neuromuscular Research, Tokyo 187-8502, Japan.
[5] Max-Planck-Institute for Heart and Lung Research, Department of Cardiac Development and Remodeling, 61231 Bad Nauheim, Germany.
[6] University of Reading, School of Biological Sciences, Reading RG6 6AH, United Kingdom.
[7] Université Paris Est Créteil, INSERM, EnvA, EFS, AP-HP, IMRB, 94010 Créteil, France.
[8] Freie Universität Berlin, Institute for Chemistry and Biochemistry, 14195 Berlin, Germany.
[9] AP-HP, Hôpital Raymond Poincaré, Service de Pédiatrie, 92380 Garches, France.

Contact info

* Correspondence: helge.amthor@uvsq.fr; amalia.stantzou@uvsq.fr

Summary (abstract)

The mechanism of pattern formation during limb muscle development remains poorly understood. The canonical view holds that naïve limb muscle progenitor cells (MPCs) invade a pre-established pattern of muscle connective tissue, thereby forming individual muscles.

Here we show that early murine embryonic limb MPCs highly accumulate pSMAD1/5/9, demonstrating active signaling of bone morphogenetic proteins (BMP) in these cells. Overexpression of inhibitory *SMAD6* in limb MPCs abrogated BMP signaling, impaired their migration and proliferation, and accelerated myogenic lineage progression. Fewer primary myofibers developed, causing an aberrant proximodistal muscle pattern. Patterning was not disturbed when *SMAD6* was overexpressed in differentiated muscle, implying that the proximodistal muscle pattern depends on BMP-mediated expansion of MPCs prior to their differentiation. We show that limb MPCs differentially express *Hox* genes, and *Hox*-expressing MPCs displayed active BMP signaling. *SMAD6* overexpression caused loss of HOXA11 in early limb MPCs. In conclusion, our data show that BMP signaling controls expansion of embryonic limb MPC as a prerequisite for establishing the proximodistal muscle pattern, a process that involves expression of *Hox* genes.

Key words

PAX3, SMAD6, BMP signaling, HOX, myogenic progenitor cell, myogenesis, muscle fiber, embryonic muscle, fetal muscle, limb muscle, patterning.

Introduction

As in all tetrapods, mammalian limb musculature is derived from a small number of myogenic progenitor cells (MPCs) that migrate from somites into the developing limb bud, where they expand in number, differentiate and form a multitude of individual muscles (Christ and Brand-Saberi, 2002). Migrating limb MPCs are thought to have no positional information but rather rely on signals from their new environment (Blagden and Hughes, 1999). The cues for muscle patterning reside in the limb mesenchymal cells and are independent of the presence of limb MPCs (Grim and Wachtler, 1991; Vallecillo-García et al., 2017). Increasing evidence suggests that individual muscles are formed when MPCs invade a prepattern that is established by muscle connective tissue (MCT) and controlled by a combination of transcription factors, e.g. HOX (Zakany and Duboule, 2007; Swinehart et al., 2013), TBX3 (Colasanto et al., 2016), TBX4/5 (Hasson et al., 2010), TCF4 (Kardon et al., 2003) and OSR1 (Vallecillo-García et al., 2017). However, the connective tissue of limbs without muscle does not form morphologically distinguishable structures that resemble the pattern of individualized muscles. The muscle-devoid space is instead filled with loosely organized mesenchyme and eventually with fat (Christ et al., 1977). Initial tendon formation occurs also independently of muscle; however, the tendons degenerate secondarily if they do not connect to a muscle (Huang et al., 2015).

Opposing the view of 'myogenic naivety', the expression of HOXA11 and HOXA13 proteins has been observed in chicken limb MPCs, suggesting that MPCs acquire positional identity. Interestingly, the spatiotemporal dynamics of HOX expression in chicken MPCs are influenced by cues emanating from the apical ectodermal ridge and the zone of polarizing activity. In addition, ectopic application of factors such as FGFs (fibroblast growth factors) and BMPs (bone morphogenetic proteins) were shown to regulate HOX expression in chicken MPCs. These findings suggest that MPCs may follow similar cues during patterning as the limb mesenchyme (Yamamoto et al., 1998; Hashimoto et al., 1999; Yamamoto and Kuroiwa, 2003).

In mice, muscle patterning starts at embryonic day (E)11.5, with successive splitting of premuscle masses into distinct blocks. Individual muscles become distinguishable from E12.5 onwards, and muscle individualization is complete by E14.5 at the end of embryonic myogenesis (Huang, 2017). Although non-muscle cells drive the limb muscle pattern (Kardon et al., 2002;

Tozer et al., 2007), MPCs first need to integrate spatiotemporal information for their appropriate positioning, proliferation and differentiation. The molecular mechanisms driving MPC proliferation and differentiation at the right place and time are not fully understood.

BMPs are involved in embryonic MPC expansion in chicken limbs (Amthor et al., 1998; Wang et al., 2010). Moreover, BMP signaling displays regionalized activity within limb fetal muscles at the muscle and tendon interface level, and fetal MPCs respond to BMP signaling in chicken limbs (Wang et al., 2010), suggesting the appositional growth of limb muscles that is maintained by direct signaling from BMP-expressing tendons. Consistent with this, BMP signaling has been recently shown to promote mesoderm-derived fibroblast transdifferentiation into myoblasts and their incorporation within fetal muscle fibers at the muscle–tendon interface (Esteves de Lima et al., 2021). However, there is a lack of formal proof for whether BMPs act directly on developing limb muscle, thereby activating a BMP-dependent cell-autonomous response, at which developmental stage this interaction takes place, whether it involves BMPs in physiological signaling in orthotopic positions and whether this impacts muscle patterning.

BMPs signal on target cells via transmembrane serine/threonine kinase receptors, which form a ligand-receptor complex that permits the phosphorylation of the type I receptor via the constitutively active type II receptor (Nohe et al., 2002; Nohe et al., 2004). The type I receptor in turn phosphorylates the BMP-responsive R-SMAD proteins 1, 5 and 9 (pSMAD1/5/9), which subsequently form complexes with co-SMAD4 and translocate into the nucleus to regulate transcriptional activity of target genes (Miyazawa and Miyazono, 2017). Upon BMP signaling, the inhibitory SMAD6 becomes upregulated as part of a negative feedback loop. SMAD6 interferes with BMP signaling by blocking R-SMAD phosphorylation at the level of the receptor, by antagonizing the pSMAD1/co-SMAD4 complex formation, and by increasing ubiquitin-mediated proteolysis of the BMP signaling components (Goto et al., 2007; Hata et al., 1998; Murakami et al., 2003).

We here explored the role of BMP signaling during mouse limb muscle development. We employed overexpression of *SMAD6* as a mean to cell-autonomously interfere with BMP signaling. We overexpressed *SMAD6* in embryonic limb MPCs and differentiated limb muscles

following Cre-induced recombination by crossing of *Rosa26*$^{LoxP\text{-}Stop\text{-}LoxP\text{-}huSMAD6\text{-}IRES\text{-}EGFP}$ mice with cre-driver mouse lines *Lbx1*^{Cre} and *HSA-Cre* (Miniou et al., 1999; Sieber et al., 2007; Stantzou et al., 2017).

Results

BMP signaling is active in limb muscle progenitors

First, we identified whether limb myogenic cells respond to BMP signaling. We monitored the nuclear accumulation of BMP-induced phosphorylated SMAD proteins using double immunofluorescence against pSMAD1/5/9 (pSMADs) and myogenic markers in mouse forelimbs at different developmental stages. In E10.5 limb buds, migrating MPCs expressed the transcription factor PAX3 **(Fig. 1)**, whereas the PAX7 and MYOD transcription factors were not detected, thus reproducing previously published data (Lepper and Fan, 2010; Wood et al., 2013). Surprisingly, all PAX3$^+$ MPCs accumulated high levels of pSMADs, whereas non-myogenic mesenchymal cells showed no or, if any, very weak levels of pSMADs **(Fig. 1)**. One day later, at E11.5, PAX3$^+$ MPCs rapidly lost BMP signaling responsiveness during lineage progression. A subset of emerging MYOD$^+$ cells were pSMADs$^+$, whereas PAX7$^+$ cells were rarely pSMAD$^+$ **(Fig. 1).**

By the end of the embryonic period, at E14.5, pSMADs were enriched at the tips of the muscle fibers abutting tendons (**Fig. S1a**). Double labeling of pSMADs with either PAX7, MYOD or myosin heavy chain (MHC) antibodies showed active BMP signaling in MYOD$^+$ myonuclei at the myotendinous junctions and notably not in tendons **(Fig. S1a)**. Low levels of pSMADs were also detected in rare PAX7$^+$ MPCs at the muscle tips **(Fig. S1a)**. By the end of the fetal period, at E18.5, the pSMAD expression pattern was reversed. Indeed, the tips of fetal muscle fibers were devoid of pSMADs, which had now accumulated in the nuclei of non-muscle cells at the muscle–tendon interface **(Fig. S1a)**. MCT cells, labeled by the marker TCF4, were rarely pSMAD$^+$ **(Fig. S1b)**. Furthermore, PAX7$^+$ and MYOD$^+$ myogenic cells occasionally accumulated pSMADs **(Fig. S1b**), consistent with the role of BMP signaling in postnatal satellite cells (Stantzou et al., 2017).

MPCs maintain myogenic fate following abrogation of BMP signaling

We abrogated BMP signaling in limb MPCs by crossing *Lbx1^{Cre}* mice (Sieber et al., 2007) with *Rosa26$^{LoxP\text{-}Stop\text{-}LoxP\text{-}huSMAD6\text{-}IRES\text{-}EGFP}$* (*RS6*) animals (Stantzou et al., 2017). In the resulting *Lbx1^{Cre};RS6* embryos, activation of the *Lbx1* promoter in migrating limb MPCs induced Cre-mediated excision of the *LoxP-Stop-LoxP* cassette, leading to the expression of the inhibitory

human *SMAD6* (*huSMAD6*) and *EGFP*. The *Lbx1^{Cre};RS6* genotype was detected at the expected frequency up to the fetal stages. However, new-born *Lbx1^{Cre};RS6* mice rarely survived, and the very few that did had severe growth retardation (data not shown). We validated the activation of the transgenes in *Lbx1^{Cre};RS6* embryos using EGFP (enhanced green fluorescent protein) as a marker of successful recombination. EGFP fluorescence was detected in cells from the proximal central field of E10.5 forelimb buds and was absent from the *RS6* controls **(Fig. S2a)**. When compared to whole-mount ISH against *Lbx1*, the position of the EGFP fluorescence corresponded to that of migrating MPCs that populated the limb mesenchyme **(Fig. S2a)**. In the forelimb buds of E12.5 *Lbx1^{Cre};RS6* embryos, EGFP was present in areas corresponding to the position of premuscle masses, as indicated by *Myod* mRNA expression **(Fig. S2a)**.

As the EGFP fluorescence was quite weak after cryosectioning, we used *Ai9* mice, a Cre recombinase-dependent tandem dimer Tomato (tdTomato) reporter strain (Madisen et al., 2010), to generate *Lbx1^{Cre};RS6/LoxP-Stop-LoxP-tdTomato* (*Lbx1^{Cre};RS6/Ai9*) embryos. All tdTomato^{+} MPCs were also positive for EGFP and for PAX3, allowing the tracing of limb MPCs, which were depleted of BMP signaling during limb mesenchyme invasion **(Fig. S2b)**. We did not find any tdTomato^{+}/EGFP^{+} MPC accumulation in somites at limb level, nor aberrant migration into the anterior/posterior/distal limb margins **(Fig. S2b)**. At E18.5, there was strong EGFP and tdTomato fluorescence in the limb muscles of *Lbx1^{Cre};RS6/Ai9* fetuses **(Fig. S2c)**. TdTomato was present in all myofibers of E18.5 forelimbs, indicating high recombination efficiency **(Fig. S2c)**. TdTomato expression was observed exclusively in developing muscles, indicating that MPCs depleted of BMP activity differentiated exclusively into muscle cells **(Fig. S2c)**.

As *Lbx1^{Cre}* represents a loss-of-function allele due to insertion of the *Cre* transgene into the *Lbx1* exon 1 coding sequence (Sieber et al., 2007), we determined whether heterozygous *Lbx1^{Cre}* mice show signs of haploinsufficiency. Myogenic marker ISH revealed similar expression pattern in *Lbx1* and *Pax3* at E10.5 or *Myod* at E11.5 in *Lbx1^{Cre}* limbs compared to that in the *RS6* controls (data not shown). We also did not find any significant difference in the total number of myofibers, and total number and density of PAX7^{+} and MYOD^{+} cells in E18.5 *Lbx1^{Cre}* limbs compared to *RS6* controls (data not shown). Furthermore, the *Lbx1^{Cre}* mice had normal viability and reproduction rates. We concluded that the loss of one functional *Lbx1* allele did not cause

haploinsufficiency, allowing us to use *RS6* and *Lbx1^{Cre}* as controls for experiments with *Lbx1^{Cre};RS6* mutants.

In summary, these results show that following Cre-recombination, the *huSMAD6-IRES-EGFP* cassette was expressed exclusively in MPCs and their progeny in developing limbs of *Lbx1^{Cre};RS6* mice, allowing permanent overexpression of the BMP signaling inhibitor SMAD6 in cells of the myogenic lineage.

SMAD6 overexpression abrogates BMP signaling and downregulates the marker genes of limb muscle development

We confirmed via RT-qPCR that *huSMAD6* was upregulated (3.7-fold) in the E18.5 forelimb muscles of *Lbx1^{Cre};RS6* fetuses compared to that of the *RS6* controls **(Fig. S2d).** Next, we determined whether *huSMAD6* overexpression caused cell-autonomous abrogation of BMP signaling in the myogenic lineage. Indeed, we observed the absence of pSMADs in PAX3^{+} MPCs in E10.5 *Lbx1^{Cre};RS6* limb buds compared to the *RS6* controls **(Fig. 2a)**. In addition, the presence of pSMADs at the tips of E14.5 muscle fibers was also lost **(Fig. 2b)**. Moreover, whole-mount ISH revealed that *Lbx1* and *Pax3* expression was strongly reduced in E10.5 *Lbx1^{Cre};RS6* limb buds compared to that in the *RS6* controls **(Fig. 2c)**. Residual *Lbx1* and *Pax3* transcripts were found in the proximal part of the limb buds. Similarly, *Myod* expression was strongly reduced in E11.5 and E12.5 limb buds from *Lbx1^{Cre};RS6* embryos compared to that from the *RS6* controls **(Fig. 2c)**. However, using ISH, we were unable to discriminate if the decreased gene expression was due to a decrease in cell number or in the transcript number per cell.

Abrogation of BMP signaling dampens limb MPC proliferation and distal migration

We transversely cryosectioned E10.5 embryos at limb level, allowing for a proximodistal sectioning plane of the developing limb bud. Double immunofluorescence for PAX3 and the proliferation marker KI67 revealed a significant reduction of the entire PAX3^{+} cell population and a decline in the PAX3^{+}/KI67^{+} subpopulation in *Lbx1^{Cre};RS6* embryos, suggesting reduced MPC proliferation after the inhibition of BMP signaling **(Fig. 3a–c)**. In addition, we analyzed the proximodistal distribution of the PAX3^{+} cell population in the E10.5 limb buds and found that the cells were significantly reduced in the middle and distal parts of the limb bud in *Lbx1^{Cre};RS6*

embryos compared to that in the *RS6* controls **(Fig. 3d, e)**. Together, these data suggest that the lack of BMP signaling in MPCs attenuated their proliferation and distal migration.

Abrogation of BMP signaling accelerates myogenesis progression of limb MPCs

In the embryonic limb, *Pax3* controls the entry of MPCs into the myogenic program (Relaix et al., 2005; Lagha et al., 2008). In E11.5 *RS6* forelimbs, we observed a transition from PAX3 to PAX7 and MYOD expression. $PAX7^+$ cells emerged in proximal pre-muscle masses **(Fig. 4a)**. $PAX3^+$ cells were located closer to the ectoderm, whereas $MYOD^+$ cells were present closer to the core of the limb bud **(Fig. 4b)**, consistent with the myogenic lineage progression from the peripheral towards central limb mesenchyme observed in developing chicken limbs (Amthor et al., 1998).

We found a precocious loss of $PAX3^+$ cells in E11.5 *Lbx1^{Cre};RS6* limbs **(Fig. 4a–c)**. The loss of $PAX3^+$ cells was accompanied by a 68% and 46% increase in total $PAX7^+$ **(Fig. 4a, d)** and $MYOD^+$ **(Fig. 4b, e)** cell numbers, respectively. In addition, the $PAX3^-/PAX7^+$ and $PAX3^-/MYOD^+$ cell population ratios increased by 68% and 61%, respectively, compared to that in the *RS6* controls **(Fig. 4f, g)**. These results suggest accelerated myogenic lineage progression in *Lbx1^{Cre};RS6* MPCs due to the absence of BMP signaling, which is similar to that shown in embryonic chicken limbs (Amthor et al., 1998).

In E12.5 *Lbx1^{Cre};RS6* limbs, the accelerated lineage progression was associated with a loss in total number of $MYOD^+$ cells (42%) and $PAX7^+$ cells (47%) **(Fig. S3a–d)**. Furthermore, we detected a decline in $PAX7^+/KI67^+$ and $PAX7^+/MYOD^+$ cell populations, whereas the proportion of $MYOD^+/MYOG^+$ cells increased, confirming the shift of myogenic lineage progression towards differentiating myoblasts at the expense of proliferating precursors **(Fig. S3b, e–g)**.

We did not observe a notable increase in cells expressing the apoptosis marker cleaved caspase-3 in the developing pre-muscle masses (data not shown). Therefore, the failure in generating limb MPCs in the absence of BMP signaling was likely caused by decreased proliferation and not apoptosis.

Abrogation of BMP signaling in MPCs disturbs *Lbx1^{Cre};RS6* limb proximodistal muscle patterning

We analyzed the consequences of decreased MPC generation on primary myofiber formation after abrogation of BMP signaling by analyzing the myofiber number in transverse sections at the end of the embryonic period (E14.5) of mouse forelimb development. The zeugopod muscles of *Lbx1^{Cre};RS6* embryos were significantly smaller and had less than half the number of primary myofibers compared to that in the *RS6* controls **(Fig. 5)**. At this stage, we observed defective muscle patterning in the *Lbx1^{Cre};RS6* embryos. Whereas muscle pattern was normal at stylopod level, certain zeugopod muscles were either completely absent (*supinator, extensor pollicis, flexor digitorum superficialis*) or fused (*extensor carpi radialis longus* and *brevis*), whereas the remaining zeugopod muscles were remarkably hypoplastic **(Fig. 5a)**. At the autopod level, only a few remnant MHC-expressing cells were observed, while autopod muscles were entirely absent **(Fig. 5a)**. The anatomical changes in muscle pattern seen at the end-embryonic stage (E14.5) persisted during the fetal stage **(Fig. 6)**.

Normal muscle patterning following abrogation of BMP signaling in differentiated muscle

We wanted to determine whether defective muscle patterning was also caused by the abrogation of BMP signaling in differentiated muscle cells. We used *HSA-Cre* driver mice to conditionally direct recombination in differentiated muscle cells. We first performed a time course to determine the spatiotemporal occurrence of HSA-Cre-driven recombination in *HSA-Cre;Ai9* crosses by following the onset of tdTomato expression. In E10.5 and E11.5 embryos, tdTomato was found in somites but not in limb buds. TdTomato was present in developing limb muscles from E12.5 onwards, which is consistent with the emergence of primary myofibers at this stage **(Fig. S2e)**. We then generated *HSA-Cre;RS6* mice to overexpress SMAD6 exclusively in terminally differentiated muscles; a mouse model we have validated previously (Stantzou et al., 2017). The forelimbs of E18.5 *HSA-Cre;RS6* fetuses developed normally, and no change was detected in the muscle pattern **(Fig. 6)**. This indicates that the information for the future muscle pattern is already present in MPCs before their differentiation. Of note, MCT did not increase

at the expense of skeletal muscle, as the pattern of collagen 12 expression in the *HSA-Cre;RS6* fetuses was similar to that of the controls despite the smaller muscles **(Fig. 6)**.

BMP signaling impacts *Hox* expression of myogenic cells

The observed changes in the muscle pattern of *Lbx1^{Cre};RS6* mutants **(Fig. 6)** resembled those previously observed in *Hoxa11/d11* double mutants (Swinehart et al., 2013), raising the question of the intrinsic positional information of myogenic cells and putative regulation by BMP signaling.

Indeed, at E10.5, PAX3^{+} MPCs, which had left the dermomyotome and migrated into the limb bud, expressed HOXA11 protein. Notably, HOXA11 levels in the MPCs were higher than in the surrounding limb mesenchymal cells **(Fig. 7a)**. As early as one day later, at E11.5, most PAX3^{+} cells had lost the high HOXA11 protein levels **(Fig. 7b)**. In the absence of BMP signaling in *Lbx1^{Cre};RS6* embryonic limbs, the MPCs failed to accumulate high levels of HOXA11 protein **(Fig. 7c compared with 7a, S4a)**.

To gain a global vision of *Hox* gene expression at single-cell resolution, we analyzed open-access single-cell RNA sequencing (scRNAseq) datasets of early chicken and mouse whole limb buds (Esteves de Lima et al., 2021; Rouco et al., 2021). Chicken and mouse limb buds have comparable *Hox* patterns in limb mesenchyme and myogenic differentiation (Pownall et al., 2002; Sundin et al., 1990; Yakushiji-Kaminatsui et al., 2018).

In chicken forelimb buds, scRNAseq showed the expression of genes of the *HOXA* and *HOXD* clusters in mesenchymal cells and in muscle cluster cells **(Fig. S4b-h and S5)**. As an example, *HOXA11* transcripts were detected in the majority (69%) of muscle cluster cells in E4 limbs (E10.5 mouse stage equivalence) and more rarely (37% of cells) by E6 (E12.5 mouse stage equivalence). In contrast, *HOXD13* transcripts were not detected before E6, where its expression was limited to a few muscle cluster cells **(Fig. S4b)**. *HOXA11* was expressed at all successive steps of the myogenic process: first in *PAX7*$^{+}$ and *MYOD*$^{+}$ MPCs at E4 and E6, and then in *MYOG*$^{+}$ myoblasts at E6 **(Fig. S4c-g)**. There was nonetheless a drop in *HOXA11* expression during myogenic lineage progression, given that at E6, 39% of *PAX7*$^{+}$ muscle cluster cells co-expressed *HOXA11*, while only 15% of *MYOG*$^{+}$ cells co-expressed *HOXA11* **(Fig. S4h)**. Interestingly, we

found a heterogeneous combinatorial expression of *HOXA* genes in single muscle cluster cells, suggesting *HOX*-dependent positional information in chicken limb MPCs **(Fig. S5a-b)**.

We next analyzed whether BMP response correlates with *HOXA* gene expression in muscle cluster cells and found that *HOXA*$^{+}$ cells (expressing one or several genes of the *HOXA* cluster) expressed BMP downstream effectors genes *ID2* and *ID3,* but not *ID1,* in higher proportion compared to *HOXA*$^{-}$ cells **(Fig. S5c-e)**. Consistently, the BMP score, which is the corrected average expression of the *ID1*, *ID2* and *ID3* genes, was significantly higher in *HOXA*$^{+}$ cells compared to *HOXA*$^{-}$ cells **(Fig. S5f)**.

scRNAseq of E12.5 mouse forelimbs showed very similar results compared to those in chicken: *i*) Muscle cluster cells expressed genes of the *Hoxa* and *Hoxd* cluster **(Fig. S6a)**; *ii*) a subset of *Hoxa11*$^{+}$ muscle cluster cells co-expressed *Pax3*, *Pax7*, *Myf5* and *Myod*, but only rarely *Myog* **(Fig. S7)**; *iii*) muscle cluster cells showed large heterogeneity in the expression of genes of the *Hoxa* cluster **(Fig. S6b)**; and iv) there was *Id1*, *Id2* and *Id3* expression in a higher proportion of *Hoxa*$^{+}$ cells than *Hoxa*$^{-}$ cells **(Fig. S6c-e)**.

Discussion

The current paradigm of limb muscle patterning considers limb MPCs naïve, where they develop individual muscles by invading a prepattern established by MCT (Kardon et al., 2003). Our results contribute to this concept by showing that BMP signaling is necessary for sufficient generation of MPCs, thereby establishing the necessary cellular source for limb muscle pattern. We used overexpression of *SMAD6* as an experimental tool to abrogate BMP signaling, which caused precocious loss of PAX3 in MPCs and accelerated myogenic lineage progression. MPCs advanced less distally, as expected, since PAX3 is a prerequisite for myogenic migration (Bober et al., 1994), likely causing a mismatch between their distal progression and the local connective tissue, and thus responsible for the observed defects in proximodistal muscle pattern.

It has been shown that impaired distal MPC migration can cause varying degrees of limb muscle defects (Brohmann et al., 2000, 1; Shin et al., 2016; Vasyutina et al., 2005). A detailed anatomical analysis of these mouse mutants would be required to determine whether different signaling cues, e.g. SF/HGF as compared to BMPs, exert distinctive roles during muscle patterning. In the absence of such comparative anatomical analysis, however, we cannot exclude the possibility that migration defects, independently of the underlying molecular mechanisms, result in a generic patterning defect.

Our data suggest that the proximodistal pattern information was already set up before MPCs differentiated and before splitting of muscle masses occurred. Indeed, muscle pattern remained normal when BMP signaling was directly abrogated in differentiated muscle. Instructions likely occurred at the early limb bud stages, which coincided with a high BMP-responsiveness of migrating PAX3^{+} MPCs. Curiously, limb MPCs, in mouse as well as in chicken, expressed *Hox* genes, suggesting that MPCs acquire positional identity at early limb bud stages. scRNAseq revealed: *i*) a high proportion of *Hox*-expressing MPCs in early limb buds; *ii*) heterogeneity of *Hox* gene expression in the MPCs; *iii*) their sequential upregulation; and *iv*) their downregulation during myogenic lineage progression. Immunohistochemistry confirmed the transcriptome data: upon leaving the dermomyotome and entering limb bud mesenchyme, PAX3^{+} migrating limb MPCs produced high HOXA11 protein levels, and this was dependent on BMP signaling. Interestingly, the *Lbx1^{Cre};RS6* mutants resembled the muscle pattern defect

observed in *Hoxa11*$^{-/-}$*/d11*$^{-/-}$ dKO mutants (Swinehart et al., 2013). We can only speculate about the role of *Hox* genes in developing muscle, and future work, such as their conditional knockout in MPCs, would be required.

Curiously, we show that MPCs were the only limb cells that showed robust BMP-dependent pSMAD expression at early limb bud stages, implying a high dependency of MPCs on BMP signaling. However, we neither explored the source of BMPs, nor which ligands of the BMP family signal to limb MPCs. In previous work in chick embryos, early migrating MPCs were found surrounded by BMP2/4/7-expressing cells at the limb margins, and ectopically applied BMP altered the positioning of premuscle masses (Amthor et al., 1998). Similar expression of BMPs in limb margins was also observed in mouse embryos (Michos et al., 2004). It remains to be determined, whether long-range BMP signaling from limb margins could regulate MPCs. Alternative sources, including expression by MPCs themselves, must be considered. Of note, triple knockout of BMP2/4/7 in the apical ectodermal ridge caused polydactyly and does not affect limb outgrowth, whereas overexpression of the BMP antagonist Gremlin in entire limb mesenchyme prevented limb outgrowth altogether (Choi et al., 2012; Norrie et al., 2014). However, muscle development has not been analysed in these mutants.

We would like to emphasize that our results support the MCT prepattern model. We believe that mesenchymal cells that form future MCT are the source of cues, including BMPs, that provide positional information to MPCs. In this scenario MCT and MPCs could be mutually dependent on each other to establish the muscle pattern. Indeed, a defined MCT pattern resembling a muscle pattern failed to develop in muscle-devoid limbs (Christ et al., 1977). Whereas tendons initially developed autonomously in lack of muscles; they degenerated secondarily (Christ et al., 1977; Schweitzer et al., 2010).

We here employed the overexpression of *SMAD6* as a mean to test the cell-autonomous effect of abrogating BMP signaling. SMAD6 inhibits Smad signaling by the BMP type I receptors ALK-3/6 subgroup and only weakly inhibits TGF-β/activin signaling via the BMP type I receptors ALK-1/2 subgroup, the latter being a preferential target of SMAD7 (Goto et al., 2007; Miyazawa and Miyazono, 2017). Since SMAD6 is not a direct component of the BMP signaling cascade,

306 further work is required to substantiate our results, such as performing specific BMP receptor
307 knockout.

308 In conclusion, our data suggest that BMP signaling controls embryonic limb MPCs to
309 maintain PAX3-expressing precursor status and to acquire positional identity by expressing HOX
310 code, thereby coordinating MPC migration and proliferation, which establishes the muscle
311 pattern prior to the splitting of premuscle masses into individual muscles.

Materials and methods

Mouse lines used for embryo generation

We conducted all animal experiments according to national and European legislation as well as institutional guidelines for the care and use of laboratory animals as approved by the French government.

The following mouse lines have been previously described: *Lbx1*^{Cre} mice (Sieber et al., 2007), *HSA-Cre* transgenic mice (Miniou et al., 1999), *Rosa26*$^{LoxP\text{-}Stop\text{-}LoxP\text{-}huSMAD6\text{-}IRES\text{-}EGFP}$ mice (i.e. *RS6*) (Stantzou et al., 2017), and *Ai9* mice, which contain an insertion in the *Rosa26* locus of a strong and ubiquitous CAG promoter, followed by a floxed-Stop cassette-controlled *tdTomato* (Madisen et al., 2010).

Lbx1^{Cre}, *HSA-Cre* and *RS6* mice were interbred to obtain *Lbx1*^{Cre}*;RS6* and *HSA-Cre;RS6* embryos. *Lbx1*^{Cre} and *Ai9* mice were interbred to obtain heterozygous *Lbx1*^{Cre}*;Ai9* mice, which were crossed with *RS6* mice to obtain *Lbx1*^{Cre}*;RS6/Ai9* embryos.

Genomic DNA isolated from ear clippings postnatally or from either yolk sacs or parts of the non-limb tissues prenatally were genotyped. The PCR primers are described in **Table S1**.

Embryonic and fetal forelimb collection and processing

Embryos and fetuses were collected in ice-cold phosphate-buffered saline (PBS) at different stages (plug date: E0.5). Embryos used for whole-mount ISH experiments were fixed overnight in 4% paraformaldehyde (PFA) at 4°C, washed twice in PBS-T (0.1% Tween-20, P9416, Sigma) and dehydrated using a methanol series of 50% methanol (15 minutes × 2) and 100% methanol (15 minutes), after which they could be stored at -20°C for whole-mount ISH.

For immunostaining, forelimbs from E10.5 and E11.5 embryos were dissected as pairs connected with the rostral (thoracic) body segment to preserve the structure of the forelimbs and forelimb-level somites. At the later stages, the forelimbs were individually dissected. The tissues were fixed at 4°C in either 1% PFA for 1 hour (E10.5–E12.5) or in 4% PFA for 2 hours (E14.5 and E18.5), washed thrice for 10 minutes and then dehydrated overnight at 4°C in either 15% sucrose (E10.5–E12.5) or 30% sucrose (E14.5 and E18.5). The forelimbs were embedded in Optimum Cutting Temperature compound (Qpath) in disposable plastic moulds (Dutscher), frozen in liquid nitrogen and stored at -80°C for sectioning.

RNA isolation and RT-qPCR

Total RNA from frozen E18.5 forelimb muscle tissue was extracted using TRIzol (Life Technologies Ambion) in combination with an RNeasy Mini kit (Qiagen). Traces of DNA in the RNA extract were removed with an RNase-Free DNase Set (Qiagen). The isolated RNA was quantified using a NanoVue Plus GE HealthCare spectrophotometer (Dutscher). Next, complementary DNA (cDNA) was synthesized using reverse transcriptase (SuperScript™ III First-Strand Synthesis SuperMix kit, Invitrogen). RT-qPCR was performed according to the SYBR Green protocol (Bio-Rad) in triplicate on a CFX96 Touch Real-Time detection system (Bio-Rad) using iTaq Universal SYBR Green Supermix (Bio-Rad) and primers for *huSMAD6* and the housekeeping gene *Gapdh* as described previously (Stantzou et al., 2017).

Whole-mount ISH

Whole-mount ISH with digoxigenin-labeled probes was used for visualizing the expression of *Lbx1*, *Pax3* or *Myod*. ISH was performed as previously described (Murgai et al., 2018)·(Tajbakhsh et al., 1997).

Immunofluorescence staining

Serial sections of frozen forelimbs on SuperFrost Plus adhesion slides (Thermo Fisher Scientific) were obtained at 10-µm thickness using a cryostat at -24°C (Leica CM3050S). E10.5 and E11.5 forelimbs were longitudinally sectioned, which allowed 2D visualization of forelimb sections in the proximodistal and dorsoventral axes. E12.5, E14.5 and E18.5 forelimbs were sectioned in the transverse plane (except stated otherwise), which allowed 2D visualization of forelimb sections in the dorsoventral and anteroposterior axes. The forelimb sections on the slides were directly used for immunofluorescence staining experiments or were stored at -80°C for future use.

Immunofluorescence staining was performed using the following protocols: *i*) 5-minute rehydration of slides in PBS; *ii*) permeabilization with 0.1% (E10.5–E12.5) or 0.5% (E14.5 and E18.5) Triton X-100 (Sigma-Aldrich) (in the case of nuclear protein staining, e.g. PAX3, PAX7, MYOD, Myogenin (MYOG), pSMAD1/5/9, HOXA11, KI67) or with methanol at -20°C (for non-nuclear proteins, e.g. MHC, laminin alpha-2, DsRed, collagen 12); *iii*) three 5-minute washes in PBS; *iv*) antigen retrieval by 20-minute immersion of the slides in boiled 10 mM citric acid

solution kept at 60°C in a water bath; the slides were cooled at room temperature in the citric acid solution, and three PBS washes were performed (only for E14.5 and E18.5 nuclear staining); *v*) up to 1.5-hour blocking with 10% normal goat serum (Abcam); *vi*) overnight incubation with primary antibodies (dilutions prepared in blocking solution, **Table S2**) at 4°C; *vii*) three 5-minute washes in PBS; *viii*) up to 1.5-hour incubation with secondary antibodies (dilutions prepared in blocking solution, **Table S2**); *ix*) three 5-minute washes in PBS; *x*) 10-minute incubation with DAPI for nuclear staining (dilution 1:5000); *xi*) 5-minute washing in PBS; *xi*i) coverslip mounting with Fluoromount-G (Southern Biotech). **Tables S2 and S3** detail the primary and secondary antibodies used in this study.

Imaging

Embryos were dissected and whole limbs in the unfixed state were immediately imaged for native EGFP and tdTomato fluorescence using a stereomicroscope (SteREO Lumar.V12, Zeiss). Native EGFP and tdTomato fluorescence was subsequently imaged on fresh unfixed cryosections, and fluorescence immunohistochemistry was captured under 20×, 40× or 63× objective using a fluorescence microscope (Zeiss Axio Imager) with an Orkan camera (Hamamatsu). Images were acquired with AxioVision software. Mosaic images of immunostained whole limbs were obtained after stitching together multiple individual images captured with a 20× objective of all the different regions in the whole limb for all fluorescence channels of interest. Masson's trichrome staining images were acquired using a digital slide scanner (Leica) and analyzed with ImageScope software. Images were exported and saved as TIFF files for further analyzes or for illustration in the figures.

Morphometric studies

The captured fluorescent images were analyzed by applying morphometric studies using ImageJ (Schneider et al., 2012).

The populations of cell and nuclear markers (PAX3, MYOD, PAX7, MYOG, KI67, HOXA11, DAPI) were quantified on immunostained cryosections as detailed above by superimposing fluorescence channels to visualize signal colocalization.

Proximodistal migration of PAX3-expressing MPCs in E10.5 forelimbs was quantified by dividing the forelimb into 10 equally sized proximodistal zones and counting the $PAX3^+$ cells in each zone.

Myofibers on the transverse sections of E14.5 forelimb zeugopods were quantified following co-immunostaining against laminin alpha-2 and MHC. Total muscle CSA was determined as the sum of the CSA of all individual zeugopod muscles.

Morphometric studies at E10.5, E11.5 and E12.5 were conducted on three consecutive sections of each forelimb, and $n = 5$ forelimbs were analyzed for each genotype except if stated otherwise. Morphometric studies at E14.5 were conducted on one transverse section through the proximal region of forelimb zeugopods, assuring measurements at the maximal size of the zeugopod muscle.

scRNAseq analysis of whole limb cells

The scRNAseq protocol for E12.5 mouse whole limb cells is described by Rouco *et al.* (Rouco et al., 2021); that for chicken whole limb cells is described by Esteves de Lima *et al.* (Esteves de Lima et al., 2021). Briefly, scRNAseq datasets were generated from whole forelimbs from two different E4 embryos and three different E6 embryos using a 10X Chromium Chip (10X Genomics) followed by sequencing with a High Output Flow Cell using an Illumina Nextseq 500 and by sequence analysis with Cell Ranger Single Cell Software Suite 3.0.2 (10X Genomics). Only mononucleated muscle cells are included in the datasets, as plurinucleated myotubes are excluded by the single-cell isolation protocol. Downstream clustering analysis of scRNAseq data was performed using the Seurat package (v3.0) (Stuart et al., 2019) under R (v3.6.1) (Macosko et al., 2015; R: The R Project for Statistical Computing). We then extracted the clusters identified as muscle clusters by the differential expression of the classical myogenic markers (*PAX7*, *MYOD*, *MYOG*) and performed the remaining analysis on these muscle clusters only. Gene expression was defined by 'gene log-normalized count > 0'. The scRNAseq datasets were analyzed using Seurat tools: FeaturePlot and Violin plots. Custom feature plots highlighting gene co-expression were generated using the R package ggplot2 v3.3.3 (Wickham, 2016). Population intersection plots were generated with the R package UpSetR v1.4.0 (Conway et al., 2017).

Within the muscle clusters, cells were grouped according to two identities, i.e. whether or not they expressed *HOXA* (*HOXA*$^{+}$ and *HOXA*$^{-}$, respectively). The *HOXA*$^{+}$ identity was defined by the expression (i.e. gene log-normalized count > 0) in a cell of at least one of the seven *HOXA* genes found in the muscle clusters (*HOXA4*, *HOXA5*, *HOXA6*, *HOXA7*, *HOXA9*, *HOXA10*, *HOXA11*). *HOXA*$^{-}$ identity was conferred to cells that expressed none of the seven *HOXA* genes. A BMP score was calculated using the AddModuleScore function for the well-characterized BMP transcriptional read-out genes *ID1*, *ID2* and *ID3*. Response to BMP signaling was then compared between these two identities using the Seurat tool Violin plots and the ggplot2 tool boxplots.

Data availability

Both chicken and mouse scRNAseq datasets have been deposited in the National Center for Biotechnology Information Gene Expression Omnibus database (https://www.ncbi.nlm.nih.gov/geo/) respectively under accession numbers GSE166981 and GSE168633.

Statistical analyses

Numerical data are presented as the mean ± standard deviation (SD). The probability for statistical differences between experimental and control groups was determined by calculating the exact *p*-value using the non-parametric two-tailed Mann-Whitney *U* test. GraphPad Prism Software version 7.00 for Windows (La Jolla, CA, USA, www.graphpad.com) was used for all statistical analyses and graphs.

Acknowledgements

We thank Prof Dr Carmen Birchmeier (Developmental Biology and Signal Transduction Group, Max Delbrück Center for Molecular Medicine, 13125 Berlin, Germany) for providing the *Lbx1*^{Cre} mice.

Declaration of interests

The authors do not have any financial or non-financial competing interests.

Funding

Financial support was provided by the Association Française contre les Myopathies (AFM) [project funding n° 20313 to H. Amthor, PhD funding n° 21357 to H. Asfour, TRANSLAMUSCLE funding n° 19507 to FR, MyoConnect funding n°22234 to D.D.], the French state through the Agence Nationale de la Recherche (ANR) [BMP-Myomass ANR-12-BSV1-0038-04 and BMP-Myostem ANR-16-CE14-0002-01 to H. Amthor, LimbCT ANR-20-CE13-0020-01 to D. Duprez, and Labex REVIVE ANR-10-LABX-73 to F.R.], the Université franco-allemande (as part of the MyoGrad International Graduate School for Myology, CDFA-06-11) to H. Amthor, and the Swiss National Science Foundation grant PP00P3_176802 to G.A..

Author Contribution

Conceptualization: H. Amthor, A.S., F.R., K.P., S. Stricker, D.D., G.A.; Methodology: H. Amthor, T.B., H. Asfour, A.S., S.H., F.Z., S. Swist, D.D., E.H., R.R., G.A.; Validation: H. Amthor, A.S., H. Asfour, D.D., E.H., R.R., G.A.; Formal analysis: H. Amthor, H. Asfour, A.S., D.D., E.H., R.R., G.A.; Investigations: H. Amthor, H. Asfour, A.S., F.Z., S.H., D.D., E.H., R.R., G.A.; Resources: H. Amthor, F.R., S. Swist, T.B., A.S., H. Asfour, D.D., E.H., R.R., G.A.; Writing-original draft preparation: H. Amthor, A.S., H. Asfour; Writing-review and editing: H. Amthor, A.S., H. Asfour, F.Z., S. Stricker, S. Swist, S.H., T.B., K.P., F.R., D.D., E.H., R.R., G.A.; Visualisation: H. Amthor, A.S., H. Asfour, R.R.; Supervision: H. Amthor, A.S., F.R., D.D., G.A.; Project administration: H. Amthor, A.S., H. Asfour; Funding acquisition: H. Amthor, H. Asfour, F.R., G.A..

References

Amthor, H., Christ, B., Weil, M. and Patel, K. (1998). The importance of timing differentiation during limb muscle development. *Curr. Biol.* **8**, 642–652.

Blagden, C. S. and Hughes, S. M. (1999). Extrinsic influences on limb muscle organisation. *Cell Tissue Res.* **296**, 141–150.

Bober, E., Franz, T., Arnold, H. H., Gruss, P. and Tremblay, P. (1994). Pax-3 is required for the development of limb muscles: a possible role for the migration of dermomyotomal muscle progenitor cells. *Development* **120**, 603–612.

Brohmann, H., Jagla, K. and Birchmeier, C. (2000). The role of Lbx1 in migration of muscle precursor cells. *Development* **127**, 437–445.

Choi, K.-S., Lee, C., Maatouk, D. M. and Harfe, B. D. (2012). Bmp2, Bmp4 and Bmp7 are co-required in the mouse AER for normal digit patterning but not limb outgrowth. *PLoS One* **7**, e37826.

Christ, B. and Brand-Saberi, B. (2002). Limb muscle development. *Int. J. Dev. Biol.* **46**, 905–914.

Christ, B., Jacob, H. J. and Jacob, M. (1977). [Experimental findings on muscle development in the limbs of the chick embryo]. *Verh Anat Ges* 1231–1237.

Colasanto, M. P., Eyal, S., Mohassel, P., Bamshad, M., Bonnemann, C. G., Zelzer, E., Moon, A. M. and Kardon, G. (2016). Development of a subset of forelimb muscles and their attachment sites requires the ulnar-mammary syndrome gene Tbx3. *Dis Model Mech* **9**, 1257–1269.

Conway, J. R., Lex, A. and Gehlenborg, N. (2017). UpSetR: an R package for the visualization of intersecting sets and their properties. *Bioinformatics* **33**, 2938–2940.

Esteves de Lima, J., Blavet, C., Bonnin, M.-A., Hirsinger, E., Comai, G., Yvernogeau, L., Delfini, M.-C., Bellenger, L., Mella, S., Nassari, S., et al. (2021). Unexpected contribution of fibroblasts to muscle lineage as a mechanism for limb muscle patterning. *Nat Commun* **12**, 3851.

Goto, K., Kamiya, Y., Imamura, T., Miyazono, K. and Miyazawa, K. (2007). Selective inhibitory effects of Smad6 on bone morphogenetic protein type I receptors. *J Biol Chem* **282**, 20603–20611.

Grim, M. and Wachtler, F. (1991). Muscle morphogenesis in the absence of myogenic cells. *Anat. Embryol.* **183**, 67–70.

Hashimoto, K., Yokouchi, Y., Yamamoto, M. and Kuroiwa, A. (1999). Distinct signaling molecules control Hoxa-11 and Hoxa-13 expression in the muscle precursor and mesenchyme of the chick limb bud. *Development* **126**, 2771–2783.

Hasson, P., DeLaurier, A., Bennett, M., Grigorieva, E., Naiche, L. A., Papaioannou, V. E., Mohun, T. J. and Logan, M. P. O. (2010). Tbx4 and Tbx5 acting in connective tissue are required for limb muscle and tendon patterning. *Dev Cell* **18**, 148–156.

Hata, A., Lagna, G., Massagué, J. and Hemmati-Brivanlou, A. (1998). Smad6 inhibits BMP/Smad1 signaling by specifically competing with the Smad4 tumor suppressor. *Genes Dev* **12**, 186–197.

Huang, A. H. (2017). Coordinated development of the limb musculoskeletal system: Tendon and muscle patterning and integration with the skeleton. *Dev. Biol.* **429**, 420–428.

Huang, A. H., Riordan, T. J., Pryce, B., Weibel, J. L., Watson, S. S., Long, F., Lefebvre, V., Harfe, B. D., Stadler, H. S., Akiyama, H., et al. (2015). Musculoskeletal integration at the wrist underlies the modular development of limb tendons. *Development* **142**, 2431–2441.

Kardon, G., Campbell, J. K. and Tabin, C. J. (2002). Local extrinsic signals determine muscle and endothelial cell fate and patterning in the vertebrate limb. *Dev. Cell* **3**, 533–545.

Kardon, G., Harfe, B. D. and Tabin, C. J. (2003). A Tcf4-positive mesodermal population provides a prepattern for vertebrate limb muscle patterning. *Dev. Cell* **5**, 937–944.

Lagha, M., Kormish, J. D., Rocancourt, D., Manceau, M., Epstein, J. A., Zaret, K. S., Relaix, F. and Buckingham, M. E. (2008). Pax3 regulation of FGF signaling affects the progression of embryonic progenitor cells into the myogenic program. *Genes Dev.* **22**, 1828–1837.

Lepper, C. and Fan, C.-M. (2010). Inducible lineage tracing of Pax7-descendant cells reveals embryonic origin of adult satellite cells. *Genesis* **48**, 424–436.

Macosko, E. Z., Basu, A., Satija, R., Nemesh, J., Shekhar, K., Goldman, M., Tirosh, I., Bialas, A. R., Kamitaki, N., Martersteck, E. M., et al. (2015). Highly Parallel Genome-wide Expression Profiling of Individual Cells Using Nanoliter Droplets. *Cell* **161**, 1202–1214.

Madisen, L., Zwingman, T. A., Sunkin, S. M., Oh, S. W., Zariwala, H. A., Gu, H., Ng, L. L., Palmiter, R. D., Hawrylycz, M. J., Jones, A. R., et al. (2010). A robust and high-throughput Cre reporting and characterization system for the whole mouse brain. *Nat. Neurosci.* **13**, 133–140.

Michos, O., Panman, L., Vintersten, K., Beier, K., Zeller, R. and Zuniga, A. (2004). Gremlin-mediated BMP antagonism induces the epithelial-mesenchymal feedback signaling controlling metanephric kidney and limb organogenesis. *Development* **131**, 3401–3410.

Miniou, P., Tiziano, D., Frugier, T., Roblot, N., Le Meur, M. and Melki, J. (1999). Gene targeting restricted to mouse striated muscle lineage. *Nucleic Acids Res.* **27**, e27.

Miyazawa, K. and Miyazono, K. (2017). Regulation of TGF-β Family Signaling by Inhibitory Smads. *Cold Spring Harb Perspect Biol* **9**, a022095.

Murakami, G., Watabe, T., Takaoka, K., Miyazono, K. and Imamura, T. (2003). Cooperative inhibition of bone morphogenetic protein signaling by Smurf1 and inhibitory Smads. *Mol Biol Cell* **14**, 2809–2817.

Murgai, A., Altmeyer, S., Wiegand, S., Tylzanowski, P. and Stricker, S. (2018). Cooperation of BMP and IHH signaling in interdigital cell fate determination. *PLoS ONE* **13**, e0197535.

Nohe, A., Hassel, S., Ehrlich, M., Neubauer, F., Sebald, W., Henis, Y. I. and Knaus, P. (2002). The mode of bone morphogenetic protein (BMP) receptor oligomerization determines different BMP-2 signaling pathways. *J Biol Chem* **277**, 5330–5338.

Nohe, A., Keating, E., Knaus, P. and Petersen, N. O. (2004). Signal transduction of bone morphogenetic protein receptors. *Cell Signal* **16**, 291–299.

Norrie, J. L., Lewandowski, J. P., Bouldin, C. M., Amarnath, S., Li, Q., Vokes, M. S., Ehrlich, L. I. R., Harfe, B. D. and Vokes, S. A. (2014). Dynamics of BMP signaling in limb bud mesenchyme and polydactyly. *Dev Biol* **393**, 270–281.

Pownall, M. E., Gustafsson, M. K. and Emerson, C. P. (2002). Myogenic regulatory factors and the specification of muscle progenitors in vertebrate embryos. *Annu Rev Cell Dev Biol* **18**, 747–783.

R: The R Project for Statistical Computing.

Relaix, F., Rocancourt, D., Mansouri, A. and Buckingham, M. (2005). A Pax3/Pax7-dependent population of skeletal muscle progenitor cells. *Nature* **435**, 948–953.

Rouco, R., Bompadre, O., Rauseo, A., Fazio, O., Thorel, F., Peraldi, R. and Andrey, G. (2021). Cell-specific alterations in Pitx1 regulatory landscape activation caused by the loss of a single enhancer. *bioRxiv* 2021.03.10.434611.

Schneider, C. A., Rasband, W. S. and Eliceiri, K. W. (2012). NIH Image to ImageJ: 25 years of image analysis. *Nat. Methods* **9**, 671–675.

Schweitzer, R., Zelzer, E. and Volk, T. (2010). Connecting muscles to tendons: tendons and musculoskeletal development in flies and vertebrates. *Development* **137**, 2807–2817.

Shin, J., Watanabe, S., Hoelper, S., Krüger, M., Kostin, S., Pöling, J., Kubin, T. and Braun, T. (2016). BRAF activates PAX3 to control muscle precursor cell migration during forelimb muscle development. *Elife* **5**,.

Sieber, M. A., Storm, R., Martinez-de-la-Torre, M., Müller, T., Wende, H., Reuter, K., Vasyutina, E. and Birchmeier, C. (2007). Lbx1 acts as a selector gene in the fate determination of somatosensory and viscerosensory relay neurons in the hindbrain. *J. Neurosci.* **27**, 4902–4909.

Stantzou, A., Schirwis, E., Swist, S., Alonso-Martin, S., Polydorou, I., Zarrouki, F., Mouisel, E., Beley, C., Julien, A., Le Grand, F., et al. (2017). BMP signaling regulates satellite cell-dependent postnatal muscle growth. *Development* **144**, 2737–2747.

Stuart, T., Butler, A., Hoffman, P., Hafemeister, C., Papalexi, E., Mauck, W. M., Hao, Y., Stoeckius, M., Smibert, P. and Satija, R. (2019). Comprehensive Integration of Single-Cell Data. *Cell* **177**, 1888-1902.e21.

Sundin, O. H., Busse, H. G., Rogers, M. B., Gudas, L. J. and Eichele, G. (1990). Region-specific expression in early chick and mouse embryos of Ghox-lab and Hox 1.6, vertebrate homeobox-containing genes related to Drosophila labial. *Development* **108**, 47–58.

Swinehart, I. T., Schlientz, A. J., Quintanilla, C. A., Mortlock, D. P. and Wellik, D. M. (2013). Hox11 genes are required for regional patterning and integration of muscle, tendon and bone. *Development* **140**, 4574–4582.

Tajbakhsh, S., Rocancourt, D., Cossu, G. and Buckingham, M. (1997). Redefining the genetic hierarchies controlling skeletal myogenesis: Pax-3 and Myf-5 act upstream of MyoD. *Cell* **89**, 127–138.

Tozer, S., Bonnin, M.-A., Relaix, F., Di Savino, S., García-Villalba, P., Coumailleau, P. and Duprez, D. (2007). Involvement of vessels and PDGFB in muscle splitting during chick limb development. *Development* **134**, 2579–2591.

Vallecillo-García, P., Orgeur, M., Vom Hofe-Schneider, S., Stumm, J., Kappert, V., Ibrahim, D. M., Börno, S. T., Hayashi, S., Relaix, F., Hildebrandt, K., et al. (2017). Odd skipped-related 1 identifies a population of embryonic fibro-adipogenic progenitors regulating myogenesis during limb development. *Nat Commun* **8**, 1218.

Vasyutina, E., Stebler, J., Brand-Saberi, B., Schulz, S., Raz, E. and Birchmeier, C. (2005). CXCR4 and Gab1 cooperate to control the development of migrating muscle progenitor cells. *Genes Dev* **19**, 2187–2198.

Wang, H., Noulet, F., Edom-Vovard, F., Tozer, S., Le Grand, F. and Duprez, D. (2010). Bmp signaling at the tips of skeletal muscles regulates the number of fetal muscle progenitors and satellite cells during development. *Dev. Cell* **18**, 643–654.

Wickham, H. (2016). *ggplot2: Elegant Graphics for Data Analysis*. 2nd ed. 2016 édition. New York, NY: Springer.

Wood, W. M., Etemad, S., Yamamoto, M. and Goldhamer, D. J. (2013). MyoD-expressing progenitors are essential for skeletal myogenesis and satellite cell development. *Dev. Biol.* **384**, 114–127.

Yakushiji-Kaminatsui, N., Lopez-Delisle, L., Bolt, C. C., Andrey, G., Beccari, L. and Duboule, D. (2018). Similarities and differences in the regulation of HoxD genes during chick and mouse limb development. *PLoS Biol* **16**, e3000004.

Yamamoto, M. and Kuroiwa, A. (2003). Hoxa-11 and Hoxa-13 are involved in repression of MyoD during limb muscle development. *Dev Growth Differ* **45**, 485–498.

Yamamoto, M., Gotoh, Y., Tamura, K., Tanaka, M., Kawakami, A., Ide, H. and Kuroiwa, A. (1998). Coordinated expression of Hoxa-11 and Hoxa-13 during limb muscle patterning. *Development* **125**, 1325–1335.

Zakany, J. and Duboule, D. (2007). The role of Hox genes during vertebrate limb development. *Curr. Opin. Genet. Dev.* **17**, 359–366.

Figures and legends

Figure 1. BMP signaling activity in developing limbs. Longitudinal sections of E10.5 and E11.5 forelimbs depict immunofluorescence signal of pSMAD1/5/9 (red) and PAX3, PAX7 or MYOD (green) following co-immunohistochemistry. Nuclei are stained with DAPI (blue). Left images show entire forelimbs, which are outlined by white dotted lines (pro: proximal; dis: distal; dor: dorsal; ven: ventral). Insets (white boxes) are shown at higher magnification on the right side of the respective entire forelimb and depict individual and merged fluorescence channels. White arrowheads show the few $PAX7^{+}$ cells positive for pSMAD1/5/9. *n* = 5 biological replicates for each immunostaining and embryonic stage. Scale bars = 200 µm.

Figure 1

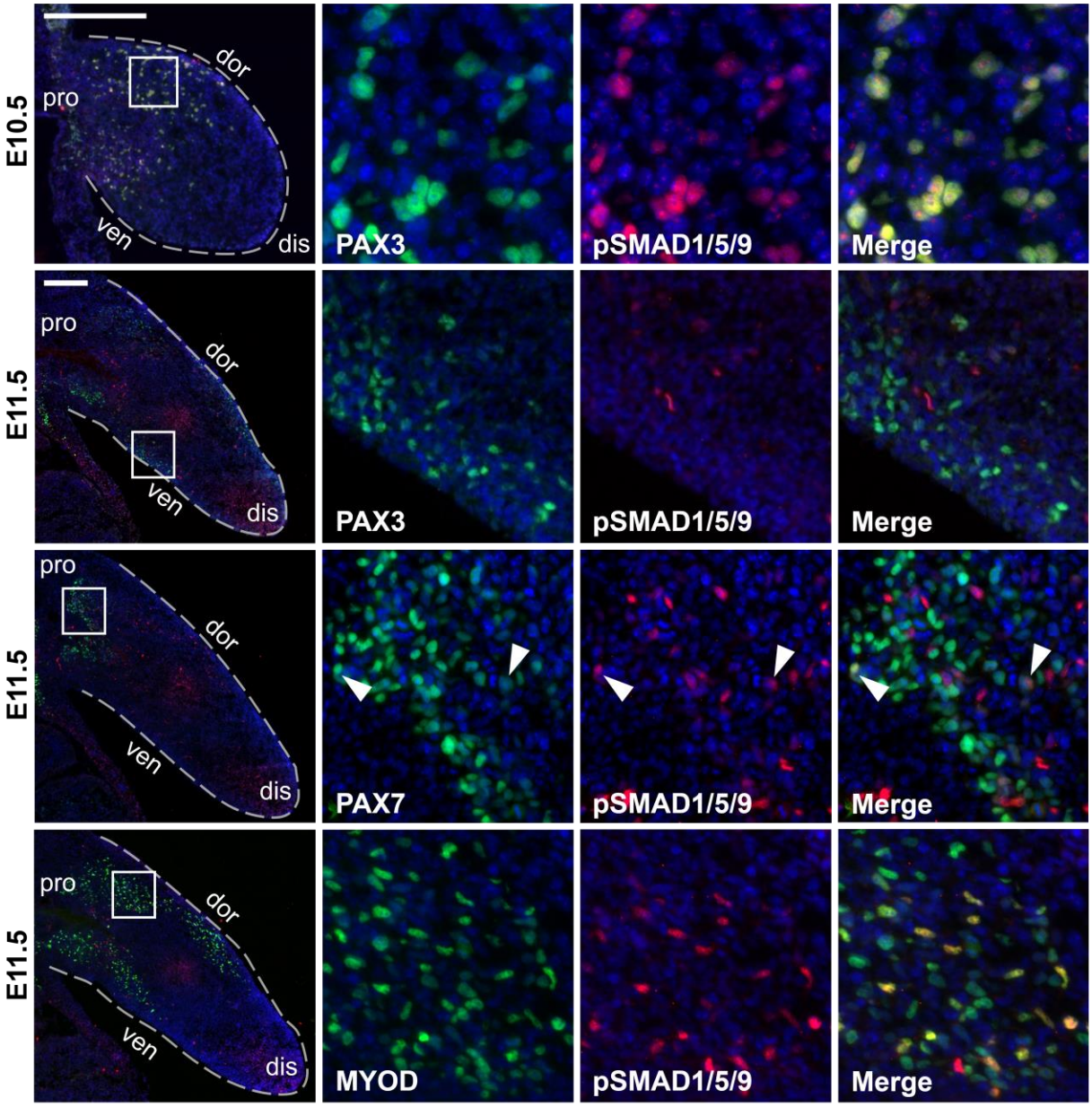
E10.5
E11.5
E11.5
E11.5
pro
dor
ven
dis
PAX3
pSMAD1/5/9
Merge
PAX7
MYOD

Figure 2. Effect of *SMAD6* overexpression in the developing limb muscles. (a-b) Effect of *SMAD6* overexpression on BMP signaling. **(a)** Left images depict the immunofluorescence signals of PAX3 (green) and pSMAD1/5/9 (red) following co-immunohistochemistry on longitudinal sections of E10.5 entire forelimbs of *RS6* and *Lbx1^{Cre};RS6* embryos. Nuclei are stained with DAPI (blue). Forelimbs are outlined by white dotted lines. Insets (white boxes) are shown at higher magnification on the right side of the respective entire forelimb and depict individual and merged fluorescence channels. **(b)** Left images depict immunofluorescence signals of MHC (green) and pSMAD1/5/9 (red) following co-immunohistochemistry on transverse sections at mid-zeugopod level of E14.5 forelimbs of *RS6* and *Lbx1^{Cre};RS6* embryos. Nuclei are stained with DAPI (blue). Insets (white solid lines) are shown at higher magnification on the right side of the respective cross-sectioned forelimb and depict the *pronator teres* muscle in individual and merged fluorescence channels. *n* = 5 biological replicates for all stages and immunostaining (pro: proximal; dis: distal; dor: dorsal; ven: ventral; ant: anterior; pos: posterior). Scale bar = 200 µm. **(c)** Effect of *SMAD6* overexpression on the transcription of early markers of limb muscle development. The images show the expression patterns of *Lbx1*, *Pax3* and *Myod* transcripts (purple) following whole-mount ISH of E10.5, E11.5 and E12.5 *Lbx1^{Cre};RS6* embryos compared to *RS6* controls. Images show dorsal view of the forelimbs (outlined by grey dotted line) (pro: proximal; dis: distal).

Figure 2

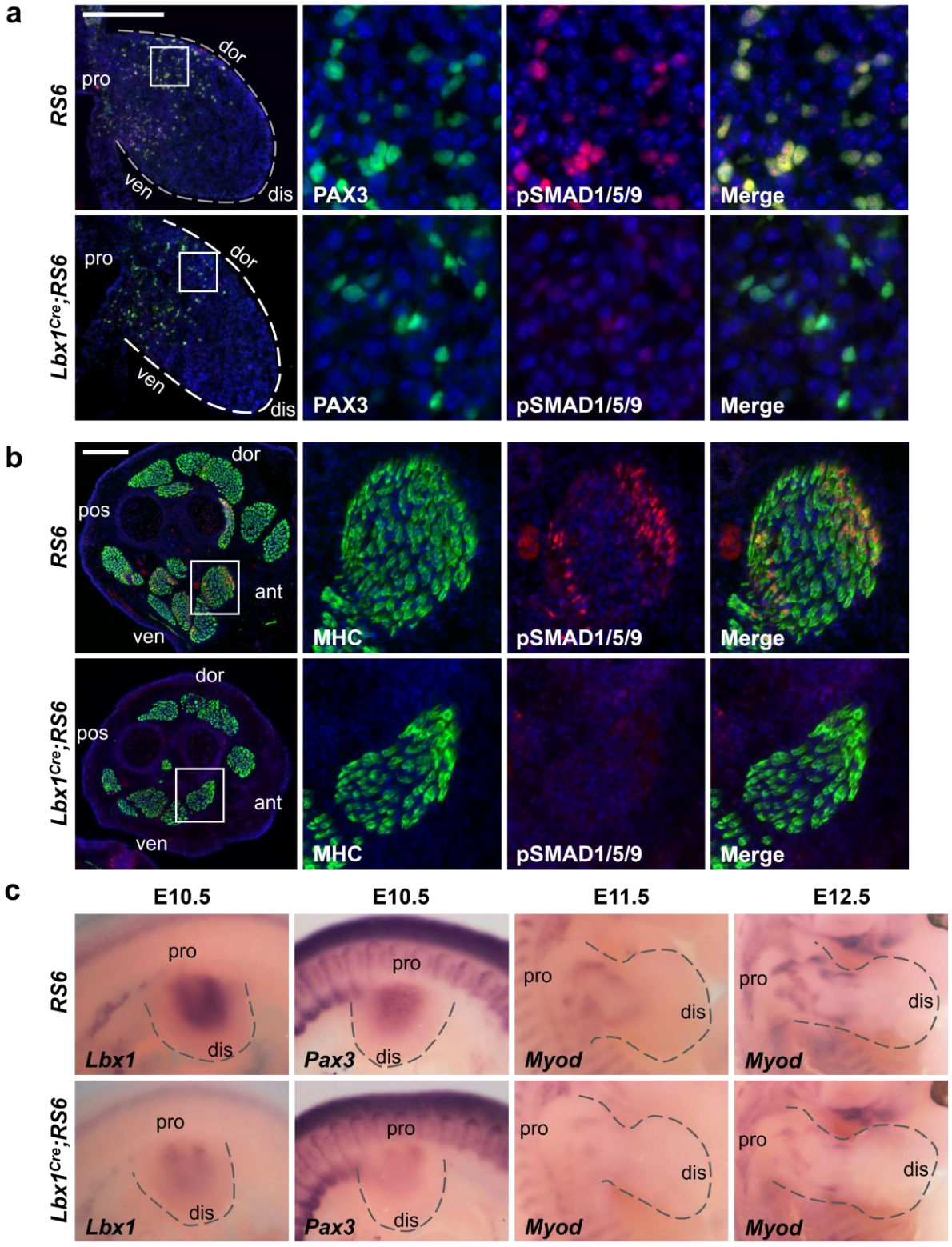
a
RS6
Lbx1Cre;RS6
pro
dor
ven
dis
PAX3
pSMAD1/5/9
Merge
b
pos
ant
MHC
c
E10.5
E10.5
E11.5
E12.5
Lbx1
Pax3
Myod

Figure 3. Effect of *SMAD6* overexpression on limb MPC proliferation and migration. (a) Left images depict immunofluorescence staining of PAX3 (green) and KI67 (red) following co-immunohistochemistry on longitudinal sections of E10.5 entire forelimbs of *RS6* control and *Lbx1^{Cre};RS6* embryos. Nuclei are stained with DAPI (blue). Insets (white solid lines) are shown at higher magnification on the right side of the respective entire forelimb and depict individual and merged fluorescence channels (pro: proximal; dis: distal; dor: dorsal; ven: ventral). Scale bar = 200 µm. **(b)** Dot-plotted bar graph shows the number of PAX3^{+} cells in the forelimbs of both genotypes. **(c)** Stacked bar graph depicts the percentages of PAX3^{+}/KI67^{+} (orange) (p = 0.0079) and PAX3^{+}/KI67^{-} (green) (p = 0.0079) MPCs in the forelimbs of both genotypes. **(d)** Immunofluorescence staining of PAX3 (green) and DAPI (blue) on longitudinal sections of E10.5 forelimbs of *RS6* control and *Lbx1^{Cre};RS6* embryos. The limb was divided into 10 equal zones along the proximodistal axis. Scale bar = 200 µm. **(e)** Histogram depicts the number of PAX3^{+} MPCs based on their position along the proximodistal limb axis as depicted in (d). n = 5 biological replicates for each genotype. Each replicate represents the mean of three consecutive serial sections. Data are the mean ± SD.

Figure 3

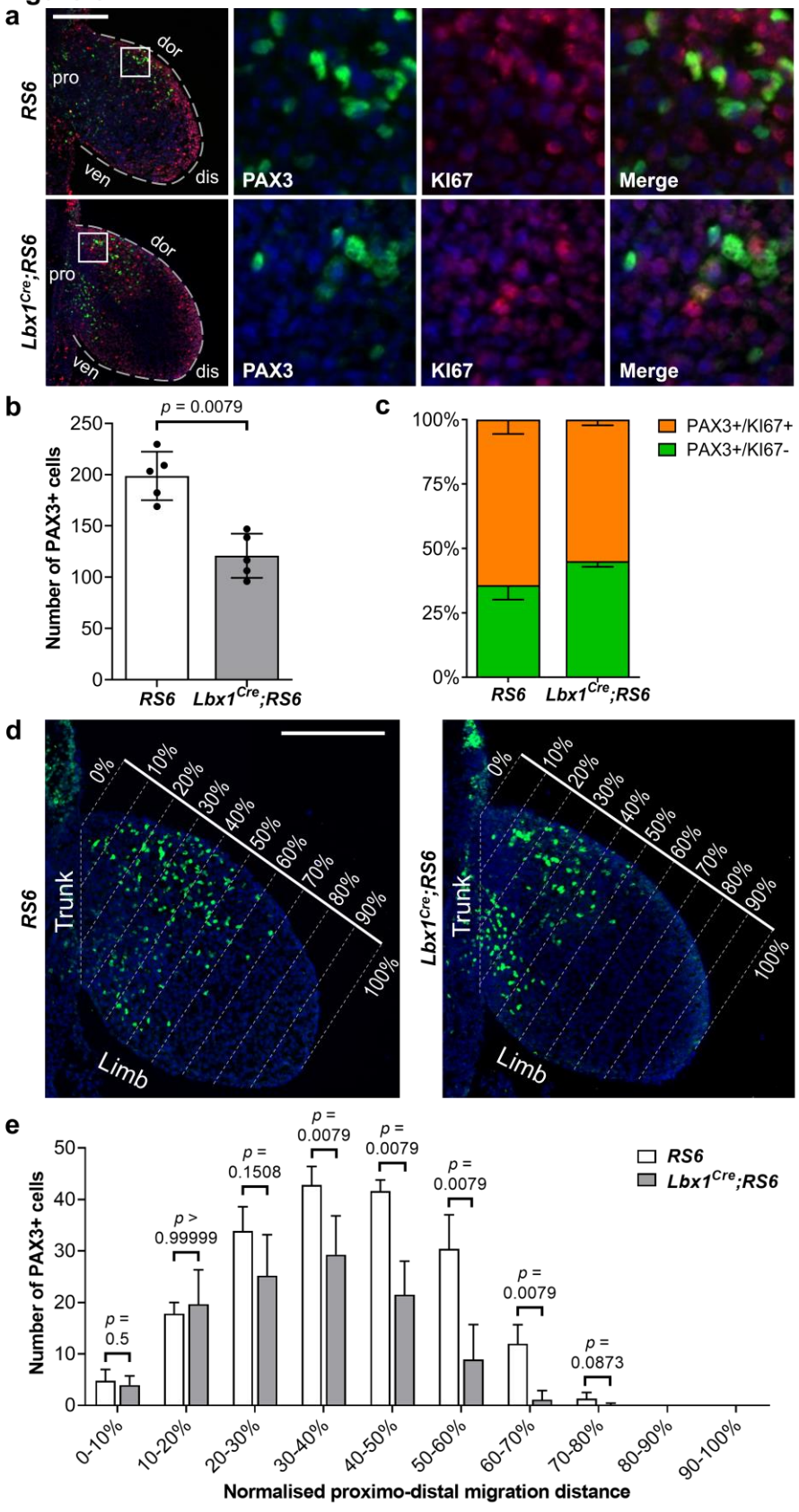
a
RS6
Lbx1Cre;RS6
pro
dor
ven
dis
PAX3
KI67
Merge
b
p = 0.0079
Number of PAX3+ cells
RS6
Lbx1Cre;RS6
c
PAX3+/KI67+
PAX3+/KI67-
d
Trunk
Limb
0%
10%
20%
30%
40%
50%
60%
70%
80%
90%
100%
e
Number of PAX3+ cells
RS6
Lbx1Cre;RS6
p = 0.5
p > 0.99999
p = 0.1508
p = 0.0079
p = 0.0079
p = 0.0079
p = 0.0079
p = 0.0873
0-10%
10-20%
20-30%
30-40%
40-50%
50-60%
60-70%
70-80%
80-90%
90-100%
Normalised proximo-distal migration distance

Figure 4. Effect of *SMAD6* overexpression on myogenic lineage progression. (a and b) Left images depict immunofluorescence staining of PAX3 (green) and either PAX7 or MYOD (red) after co-immunohistochemistry on longitudinal sections of E11.5 entire forelimbs of *RS6* control and *Lbx1^{Cre};RS6* embryos. Nuclei are stained with DAPI (blue). Limbs are outlined by white dotted lines (pro: proximal; dis: distal; dor: dorsal; ven: ventral). Scale bar = 200 µm. Insets (white boxes) are shown at higher magnification on the right side of the respective entire forelimb and depict individual and merged fluorescence channels. **(c–e)** Dot-plotted bar graphs show the total number of PAX3^{+}, PAX7^{+} and MYOD^{+} cells. **(f)** Stacked bar graph depicts the percentages of PAX3^{+}/PAX7^{-} cells (green) (p = 0.0159), PAX3^{+}/PAX7^{+} cells (orange) (p = 0.1905) and PAX3^{-}/PAX7^{+} cells (red) (p = 0.0159). **(g)** Stacked bar graph depicts the percentages of PAX3^{+}/MYOD^{-} cells (green) (p = 0.0159), PAX3^{+}/MYOD^{+} cells (orange) (p = 0.0159) and PAX3^{-}/MYOD^{+} cells (red) (p = 0.0159) cells. n = 4 biological replicates for *RS6* and n = 5 for *Lbx1^{Cre};RS6*. Each replicate represents the mean of three consecutive serial sections. Data are the mean ± SD.

Figure 4

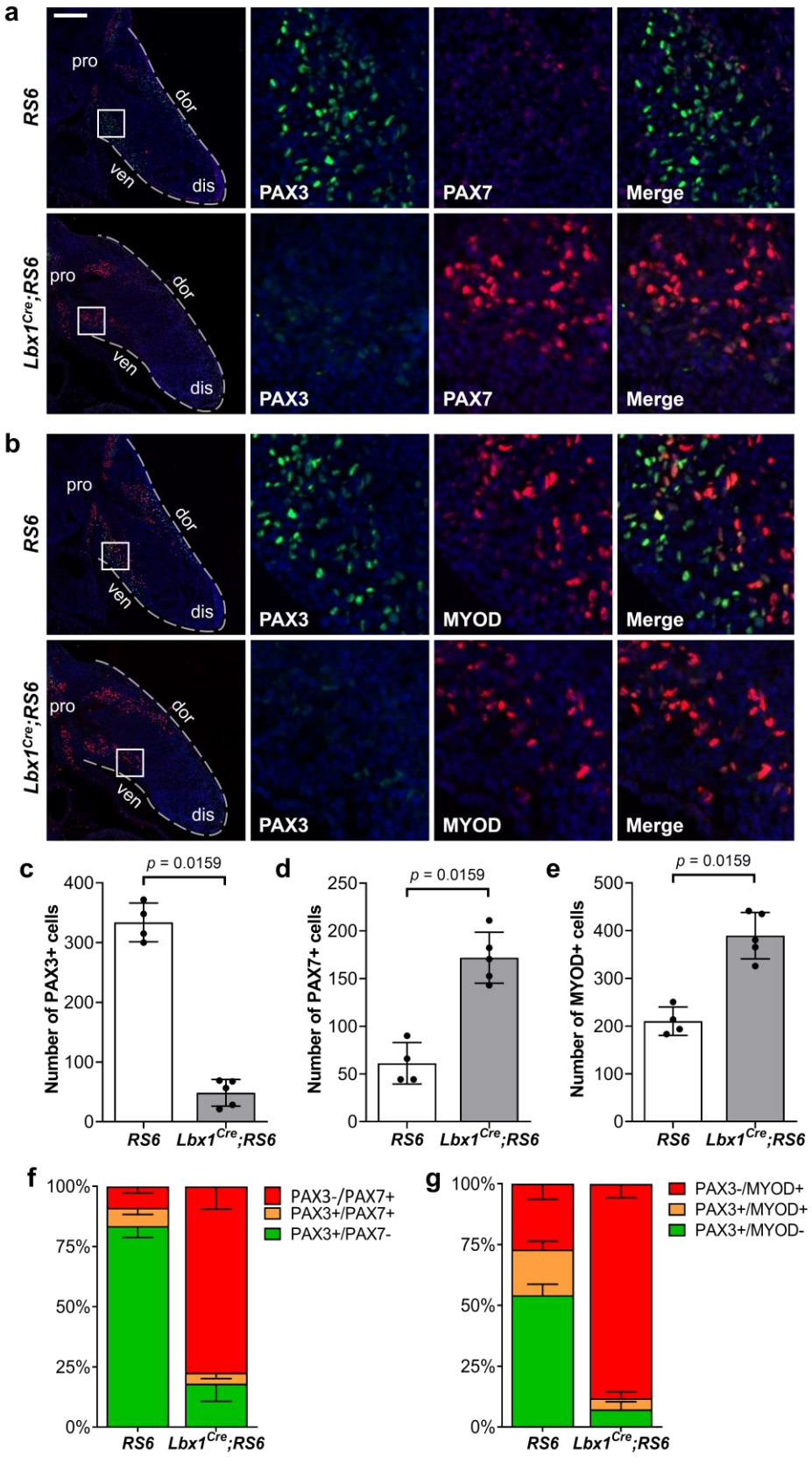
a
RS6
Lbx1Cre;RS6
pro
dor
ven
dis
PAX3
PAX7
Merge
b
MYOD
c
Number of PAX3+ cells
d
Number of PAX7+ cells
e
Number of MYOD+ cells
p = 0.0159
RS6
Lbx1Cre;RS6
f
PAX3-/PAX7+
PAX3+/PAX7+
PAX3+/PAX7-
g
PAX3-/MYOD+
PAX3+/MYOD+
PAX3+/MYOD-
100%
75%
50%
25%
0%

Figure 5. Effect of *SMAD6* overexpression on embryonic muscle pattern. (a) Immunostaining for MHC (red) on transverse sections at the zeugopod (upper images) and autopod (lower images) level of E14.5 forelimbs from *RS6* and *Lbx1^{Cre};RS6* embryos. Nuclei are stained with DAPI (blue). Inset (yellow dotted lines) is shown at higher magnification to depict remnants of MHC-expressing cells in the *Lbx1^{Cre};RS6* forelimb autopod. Muscles, which are numbered in yellow in *RS6* embryos, are absent from the *Lbx1^{Cre};RS6* embryos (yellow asterisks). Letters indicate the bones: r: *radius*; u: *ulna*; m: *metacarpals*. Numbers indicate the muscles: 9: *extensor carpi radialis longus*; 10: *extensor carpi radialis brevis*; 11: *extensor digitorum communis*; 12: *extensor digitorum lateralis*; 13: *extensor carpi ulnaris*; 14: *supinator*; 15: *extensor pollicis*; 16: *extensor indicis proprius*; 17: *pronator teres*; 18: *flexor carpi radialis*; 19: *palmaris longus*; 20: *flexor carpi ulnaris*; 21: *flexor digitorum superficialis*; 22/23/24/25: *flexor digitorum profundus* (superficial 's', humeral 'h', ulnar 'u' and radial 'r' heads); 26: *pronator quadratus*; 27: *thenars*; 28: *hypothenars*; 29: *lumbricals*; 30: *interossei*. Scale bar = 200 µm. **(b and c)** Dot-plotted bar graphs show CSA **(b)** and total myofiber number **(c)** of zeugopod muscles of both genotypes at E14.5. The muscle CSA measurement and myofiber count were conducted on transverse sections at the proximal zeugopod level. *n* = 5 biological replicates. Data are the mean ± SD.

Figure 5

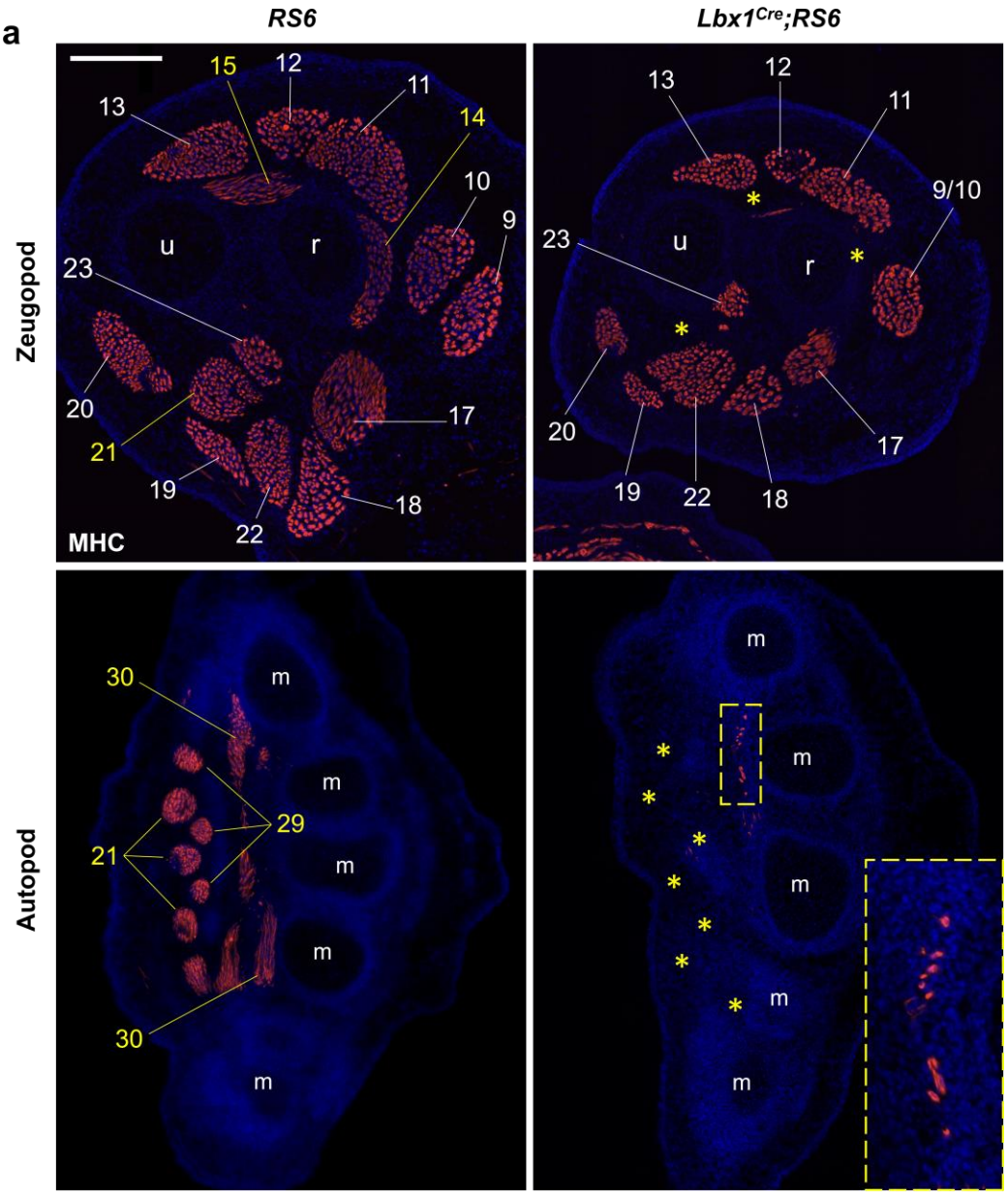
a
RS6
Lbx1Cre;RS6
Zeugopod
Autopod
MHC
15
12
11
13
14
10
9
u
r
23
20
21
19
22
18
17
9/10
m
30
29
b
CSA of zeugopod muscles (mm²)
p = 0.0079
0.25
0.20
0.15
0.10
0.05
0.00
RS6
Lbx1Cre;RS6
c
Number of zeugopod myofibres
p = 0.0079
2500
2000
1500
1000
500
0
RS6
Lbx1Cre;RS6

Figure 6. Effect of *SMAD6* overexpression on fetal muscle pattern. Immunostaining for MHC (red) and collagen 12 (green) on transverse sections at the zeugopod (upper images) and autopod (lower images) level of E18.5 forelimbs from *RS6*, *Lbx1^{Cre};RS6* and *HSA-Cre;RS6* embryos. Row 1 and 3 show merged images; row 2 and 4 show collagen 12. Muscles, which are numbered in yellow in *RS6* embryos, are absent from the *Lbx1^{Cre};RS6* embryos (yellow asterisks). Letters indicate the bones: r: *radius*; u: *ulna*; m: *metacarpals*. Numbers indicate muscles as well as the corresponding MCT compartments and tendons: 9: *extensor carpi radialis longus*; 10: *extensor carpi radialis brevis*; 11: *extensor digitorum communis*; 12: *extensor digitorum lateralis*; 13: *extensor carpi ulnaris*; 14: *supinator*; 15: *extensor pollicis*; 16: *extensor indicis proprius*; 17: *pronator teres*; 18: *flexor carpi radialis*; 19: *palmaris longus*; 20: *flexor carpi ulnaris*; 21: *flexor digitorum superficialis*; 22/23/24/25: *flexor digitorum profundus* (superficial 's', humeral 'h', ulnar 'u' and radial 'r' heads); 26: *pronator quadratus*; 27: *thenars*; 28: *hypothenars*; 29: *lumbricals*; 30: *interossei*. Scale bar = 500 µm. *n* = 5 biological replicates.

Figure 6

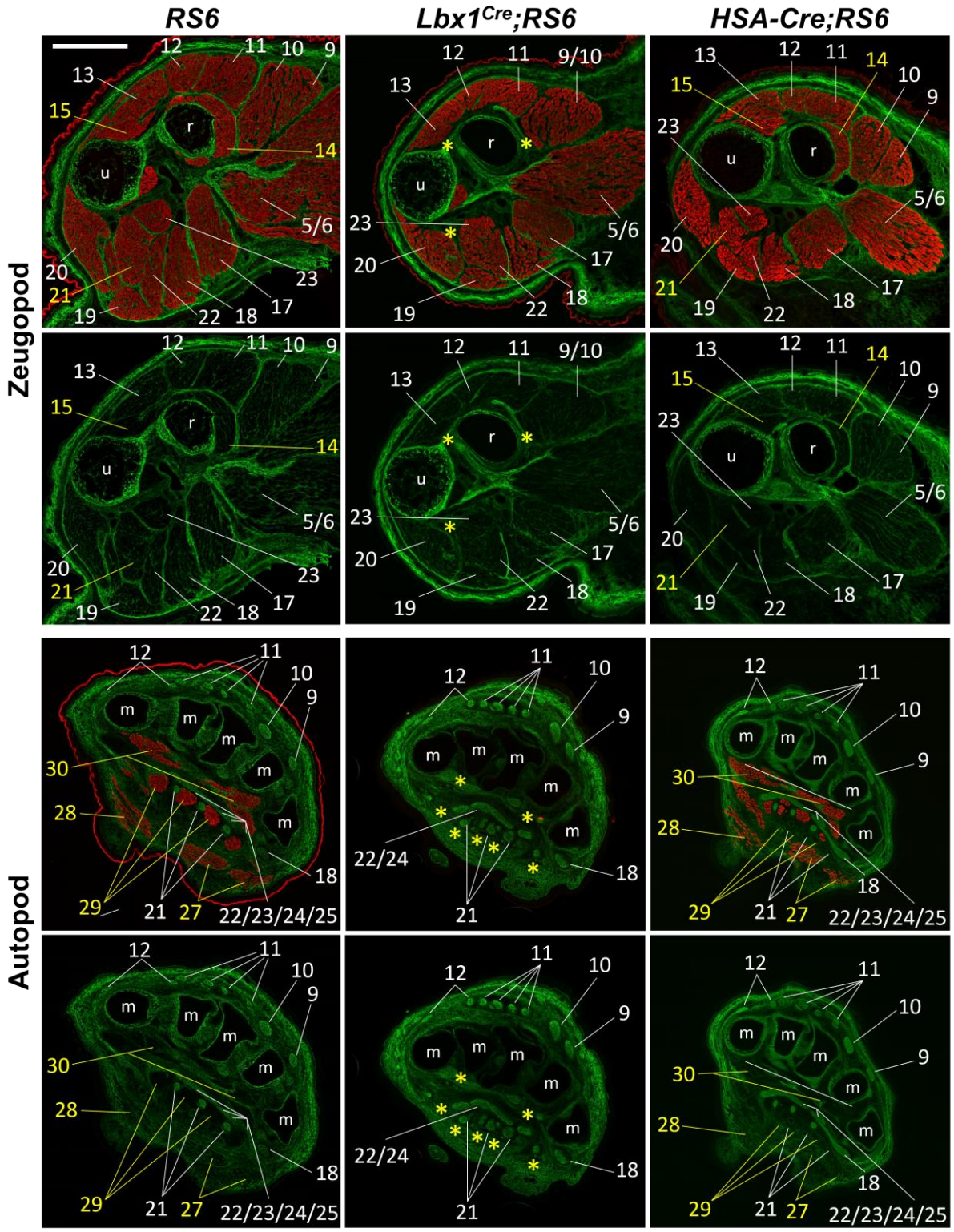
RS6
Lbx1Cre;RS6
HSA-Cre;RS6
Zeugopod
Autopod
r
u
m
12
11
10
9
9/10
13
14
15
5/6
23
20
21
19
22
18
17
30
28
29
27
22/23/24/25
22/24

Figure 7. HOX proteins in MPCs relies on BMP signaling. Co-immunohistochemistry of longitudinal sections of embryonic limbs. Forelimbs are outlined by white dotted lines. Insets (white boxes) are shown at higher magnification on the right side of the respective entire forelimb and depict individual and merged fluorescence channels. (pro: proximal; dis: distal; dor: dorsal; ven: ventral). **(a)** PAX3 (green) and HOXA11 (magenta) of control *RS6* forelimbs at E10.5. Insets depict representative *RS6* forelimb MPCs highly positive for HOXA11. White arrowhead indicates ventral lip of the dermomyotome. **(b)** PAX3 (green) and HOXA11 (magenta) of *RS6* forelimbs at E11.5. Insets depict a portion of the mid-ventral pre-muscle mass. White arrowheads indicate the few $PAX3^{+}$ cell remaining positive for HOXA11. **(c)** PAX3 (green) and HOXA11 (magenta) of *Lbx1Cre;RS6* forelimbs at E10.5. Insets depict representative *Lbx1Cre;RS6* forelimb MPCs weakly positive for HOXA11. Scale bars = 200 µm. *n* = 4-5 biological replicates for *RS6* limbs and *n* = 5 for $Lbx1^{Cre};RS6$ limbs.

Figure 7

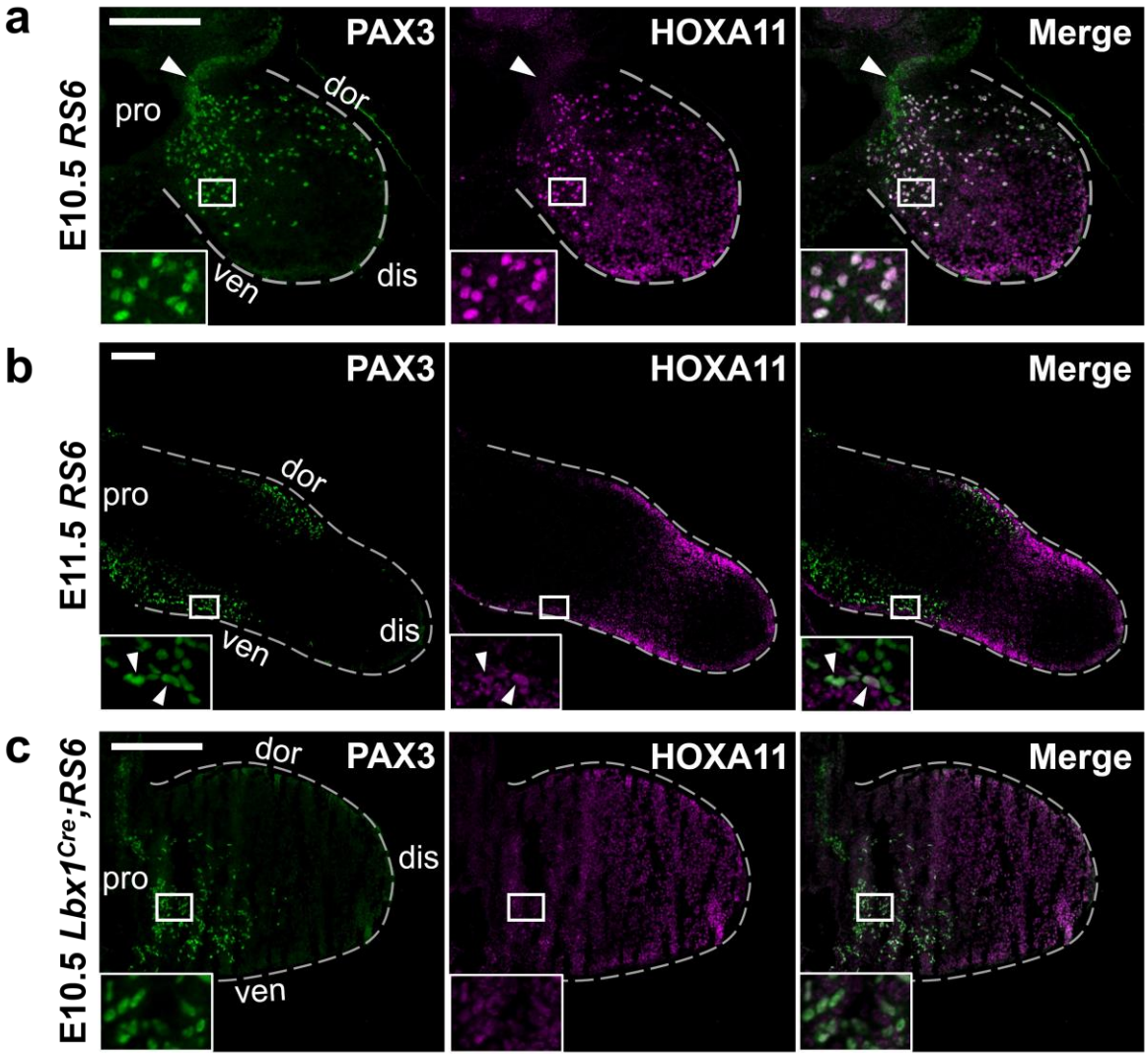
a
E10.5 RS6
PAX3
HOXA11
Merge
pro
dor
ven
dis
b
E11.5 RS6
PAX3
HOXA11
Merge
pro
dor
ven
dis
c
E10.5 Lbx1Cre;RS6
PAX3
HOXA11
Merge
dor
pro
dis
ven

472